Role of the Metal-Support Interface in the Hydrodeoxygenation Reaction of Phenol

Camila A. Teles[1,2], Raimundo C. Rabelo-Neto[1], Nhung Duong[3], Jhon Quiroz[4], Pedro H. C. Camargo[4], Gary Jacobs[5,6], Daniel E. Resasco[3], Fábio B. Noronha[1,2,*]

[1] National Institute of Technology, Catalysis Division, Rio de Janeiro, 20081-312, Brazil.

[2] Military Institute of Engineering, Chemical Engineering Department, Praça Gal. Tibúrcio 80, Rio de Janeiro, 22290-270, Brazil.

[3] Center for Biomass refining, School of Chemical, Biological and Materials Engineering, The University of Oklahoma, Norman, OK, 73019, USA.

[4] Department of Chemistry, University of Helsinki, A.I. Virtasen aukio 1, Helsinki, Finland.

[5] University of Texas at San Antonio, Department of Biomedical Engineering and Chemical Engineering, 1 UTSA Circle, San Antonio, TX 78249 USA.

[6] University of Texas at San Antonio, Department of Mechanical Engineering, 1 UTSA Circle, San Antonio, TX 78249 USA.

* Corresponding author: fabio.bellot@int.gov.br

Submitted to

Applied Catalysis B: Environmental

Revised June 2020

Abstract

In this work, the effect of interfacial sites between Pd particles and Nb_2O_5 species is investigated by testing a series of Pd-Nb_2O_5/SiO_2 catalysts with different niobium loadings for the HDO reaction of phenol in the gas phase. Important differences in the selectivity to deoxygenated product were observed depending on the presence of niobium oxide close to Pd particles, which reveals the key role of the type of active phase in the control of reaction steps. It was found that Pd/SiO_2 catalyst promotes hydrogenation pathways, producing cyclohexanone as the major product. For Pd-Nb_2O_5/SiO_2 catalyst containing a Nb/Pd molar ratio of 0.5, a sharp increase in the selectivity to benzene is observed (7.5-fold). Increasing the Nb/Pd molar ratio, the formation of benzene is enhanced. The results showed that the Pd-Nb_2O_5 interface, composed by an oxophilic oxide in the perimeter of the metal particle, is responsible for the activation of the C-O bond, promoting the deoxygenation reaction.

Keywords: Bio-oil; Hydrodeoxygenation; Phenol; metal-support interface; niobia**.**

1. Introduction

The hydrodeoxygenation (HDO) of phenolic compounds is currently used to study the mechanism of oxygen removal from bio-oil derived compounds produced on the pyrolysis of lignocellulosic biomass.

Three different reaction pathways for HDO reaction of phenolic molecules such as phenol have been reported in the literature: (i) hydrogenation of the aromatic ring producing cyclohexanol followed by its dehydration [1-6]; (ii) direct deoxygenation by cleavage of the C_{sp2}-O bond [7-16]; and (iii) tautomerization of phenol producing a keto tautomer intermediate in which the aromatic ring is hydrogenated to cyclohexanone and then cyclohexanol, or the C=O bond is hydrogenated producing an unsaturated alcohol which is rapidly converted to benzene via dehydration [17-27]. Due to this variety in reaction mechanisms, the nature of the active site remains unclear. It is generally accepted that a bifunctional catalyst is required for HDO of phenolic compounds, in which the hydrogenation over a metallic site is followed by the sequential dehydration/deoxygenation over the support. However, the role of the support and the metal-support interface is under debate. For instance, some authors propose that the deoxygenation reaction takes place on the acid sites [1-6] whereas others suggest that the defect sites of the support are responsible for the deoxygenation activity [28,29].

Recently, it has been demonstrated that supports containing oxophilic sites promote the formation of deoxygenated products [20,30-37]. It has been shown that supports such as ZrO_2, TiO_2 and Nb_2O_5 promote the deoxygenation via hydrogenation of C=O bond of the produced tautomer [20,30-33]. Among the studied catalysts, the one supported on niobium exhibited the highest selectivity towards the deoxygenated product, benzene. This enhanced selectivity is likely due to the strong interaction of the oxygen atom from phenol molecule with the Nb^{5+}/Nb^{4+} cations, yielding benzene by

hydrogenation of the C=O bond of the keto tautomer or by direct dehydroxylation of phenol.

Xi et al.[38] and Xia et al. [39] also reported outstanding performance of Pt or Pd supported on $NbOPO_4$ as catalysts for the deoxygenation of different oxygenated model compounds (sorbitol and furan-derived adducts). Experimental and theoretical studies demonstrated that NbO_x species play a key role in C-O bond cleavage [39]. As a multifunctional catalyst, $Pd/NbOPO_4$ has multiple roles in the reaction: (i) Pd metal is the active center for hydrogenation; (ii) NbO_x species promote the activation and cleavage of the C-O bond and (iii) the acid sites catalyze dehydration steps.

These previous reports evidenced the importance of active sites at the interface between two different materials that have different properties. The interplay between the metal and the support interface for the HDO reactions can potentially boost or even open specific reaction pathways that are otherwise hindered in single site catalysts.

For instance, Zhang et al. [40] encapsulated Pd nanoparticles with TiO_2 films of regulated porosity to produce interfacial sites resulting in a high selectivity toward the deoxygenated products for the HDO reaction of furfuryl alcohol, benzyl alcohol, furfural and m-cresol. These results were attributed to a combined effect of controlling binding orientation of the reactants and the presence of metal-support interfacial sites. By a combination of theory and experiments, Omotoso et al. [25] investigated the nature of active sites for the deoxygenation of m-cresol to toluene over Ru/TiO_2 catalysts with different metal loading, particle size and support phase. They showed that the site responsible for the direct cleavage of C-O bond of m-cresol molecule is the perimeter of the metal particle around the TiO_2 support. By changing the particle size of Ru, a correlation between the rate of HDO and Ru perimeter was obtained. Furthermore, DFT

calculations showed that the activation barrier for C-O cleavage is significantly reduced at an interfacial site as compared to the Ru surface (0.7 eV and 1.4 eV, respectively).

In this work, we address the role of the metal-support interface on the HDO reaction of phenol by using a Pd-Nb_2O_5 system deposited on a silica surface. The effect of Nb content was also investigated, and the resulting catalysts were evaluated for the HDO reaction of phenol in gas phase at 573 K and atmospheric pressure.

2. Experimental Section

2.1. Catalyst Preparation

The SiO_2 used as support (silica gel, Aldrich, 7631-86-9) was calcined under air flow (50 mL/min) at a heating rate of 5 K/min up to 1073 K, remaining at this temperature for 5 h. Nb_2O_5 support was obtained by calcination of niobic acid (CBMM) under air flow (50 mL/min) at 5 K/min up to 673 K for 4 h.

The Pd/SiO_2 and $PdNb/SiO_2$ catalysts were prepared by wet impregnation of SiO_2 with an aqueous solution of $Pd(NO_3)_2.2H_2O$ (20 wt% Pd in nitric acid, Umicore) and ammonium niobium oxalate ($NH_4[NbO(C_2O_4)_2(H_2O)_2].nH_2O$ – CBMM) in a rotary evaporator. The concentration of palladium nitrate and ammonium niobium oxalate in the solution were 6.7 g/L and 2.3 - 44.8 g/L (depending of the desired Pd/Nb molar ratio), respectively. The solution was maintained at 298 K under continuous stirring for 24 h. Then, the solvent was removed by evaporation under reduced pressure at 373 K. The solid was dried in air at 293 K for 12 h and then calcined under synthetic air flow (50 mL/min) at 673 K for 3 h (2 K/min). The catalysts were prepared in order to obtain 2 wt.% of Pd and different Pd:Nb molar ratios, 1:0; 1:0.5; 1:1; 1:2.5, 1:5 and 1:10. Pd/Nb_2O_5 catalyst was prepared by incipient wetness impregnation of the niobia (pore volume = 0.5 mL/g) with an aqueous solution of $Pd(NO_3)_2.2H_2O$. After impregnation, the powder was dried and then calcined using similar conditions described before.

2.2. Catalyst Characterization

Specific surface areas of the samples were measured using a Micromeritics ASAP 2020 analyzer by N_2 adsorption at the boiling temperature of liquid nitrogen.

The density of acid sites of the catalysts was measured by temperature-programmed desorption of ammonia (NH_3-TPD) and by using the cyclohexanol

dehydration probe reaction [41]. For NH_3-TPD experiments, the samples (400 mg) were reduced at 573 K for 1 h under flowing H_2 (60 mL/min) and then purged under He flow for 30 min. After reduction, the sample was cooled to 423 K and the He flow was switched to a mixture containing 4% NH_3 in He (30 mL/min) for 30 min. The physisorbed ammonia was flushed out with flowing He for 1 h. Then, the catalyst was heated at 20 K/min under He to 773 K. The cyclohexanol dehydration reaction was performed using a quartz fixed-bed reactor at 1 atm and 513 K. The fresh catalysts were previously reduced with hydrogen (60 mL/min) at 573 K for 1 h and then purged in He flow for 30 min. The reaction mixture was obtained by flowing He (100 mL/min) through a saturator containing cyclohexanol, which was kept at 336 K. The reaction products were analyzed using an Agilent Technologies 7890 GC, equipped with a HP-Innowax capillary column and a flame-ionization detector (FID). The dehydration reaction rate was calculated based on the yield of cyclohexene produced.

Diffuse reflectance spectra (DRS) were obtained with a Shimadzu UV-2600 spectrophotometer equipped with an integrating sphere (ISR-2000, Shimadzu) using $BaSO_4$ as the reflectance standard sample. All spectra were obtained in a wavelength range of 200 to 800 nm. The reflectance data are reported as the Kubelka-Munk function $F(R_\infty)$ versus the wavelength. Band gap energy was determined by the interception of the straight line fitted through the low energy side of the curve $[F(R_\infty).h\nu]^2$ versus *hν* (eV) with the X axis.

High resolution transmission electron microscopy (HRTEM) and energy dispersive X-ray spectroscopy (EDX) analyses were acquired using a FEI TECNAI G2 F20 operated at 200 kV. Prior to TEM observations, the sample was dispersed in ethanol using an ultrasound bath for 15min and deposited onto a holey-carbon copper grids, followed by drying under ambient conditions. The average diameter of the

resulting Pd supported nanoparticles was estimated by individually measuring the diameter of 200 nanoparticles. The compositional analysis was obtained from an EDX sum spectrum.

In situ X-Ray powder diffraction (XRD) measurements were performed at the XRD1-D12A beamline of the Brazilian Synchrotron Light Laboratory (LNLS), Campinas, Brazil [42]. The sample was loaded into a quartz capillary of 1.0 mm diameter between two quartz wool beds. The capillary was placed in a reaction cell connected to a 3-circle Heavy Duty diffractometer from Newport® and oriented horizontally and perpendicularly to the X-ray beam. A Yaskawa-Motoman robotic arm was used to hold a hot air blower above the sample to control the temperature during the experiment. The diffraction patterns in a 2θ range between 10 and 120° with an acquisition time of 150 s were obtained using an array of 24 Mythen (Dectris®), installed in the delta circle at 760 mm from the sample. The wavelength of $\lambda = 1.0332$ Å was selected by a double-crystal Si (111) monochromator. λ and the distance of the sample to the detector were calibrated using Si (SRM 640d) and Al_2O_3 (SRM 676a) powders NIST standards. The measurements were carried out while the sample underwent the following treatments: (i) under a flow of He (8 mL/min) at 298 K: (ii) under a 5% H_2/He mixture flow at 298 K, and (iii) under a 5% H_2/He mixture flow from 298 to 573 or 773 K at a heating of 10 K/min, remaining at this temperature for 1 h. The average crystallite size of metallic Pd under different treatments was calculated using the Scherrer equation and the line characteristic of Pd^0 (111) at $2\theta = 26.5°$.

In situ X-Ray absorption spectroscopy (XAS) experiments at the Pd K-edge (E_0 = 24.350 keV) and Nb K-edge (E_0 = 18.986 keV) were performed at the XDS-W09A beamline [43] of the Brazilian Synchrotron Light Source (LNLS, Campinas - Brazil). Typically, wafers containing pressed mixtures of the sample with boron nitride as a

binder were then placed into a sample holder located inside a quartz tubular reactor, and temperature was controlled by a furnace. The XAS experiments were recorded while the sample underwent the following treatment: (i) under He flow (50 mL/min) at 298 K; (ii) under a flow of 5% H_2/He mixture (50 mL/min) at 298 K; (iii) after reduction at 573 K for 1h at a heating rate of 10 K/min and purged with helium at the same temperature for 30 min; (iv) and cooling to 298 K under a He flow (50 mL/min). The extraction of the (k) function has been performed using the ATHENA software package. EXAFS data analysis was performed using Athena and Artemis software [44]. EXAFS R-space fitting was performed considering the amplitudes and phase shifts generated from the scattering paths through the first coordination shell of references Pd foil. Data fitting allowed the estimation of the structural parameters N, R and σ_{dw}, which are the average number of neighbouring scatterers around the absorber atom, the interatomic bond lengths and the Debye-Waller factor, respectively.

Temperature-programmed oxidation (TPO) experiments were carried out to investigate the formation of carbon after the long-term HDO reaction. TPO experiments were performed in a micro-reactor coupled to a quadrupole mass spectrometer (Gas analysis – Prisma QME200/Pfeiffer). After the HDO of phenol reaction (long-term reaction, 7 h), the reactor temperature was kept at 573 K, flushed in He for 30 min and then cooled to room temperature. Then, the samples were heated up to 1173 K at a rate of 10 K/min under a 20% O_2:He mixture (30 mL/min).

In order to probe the reaction mechanism, DRIFTS experiments were conducted using a Nicolet Nexus 870 instrument with a DTGS-TEC detector and a Thermo Spectra-Tech reaction chamber with ZnSe windows, using the conditions representative of HDO. The Pd/Nb_2O_5 sample (~ 40 mg) were first reduced under H_2 (60 mL/min) at 573 K, purged with He flow and the temperature was decreased to 323 K to record a

background spectrum. Then, helium was passed through a saturator containing phenol at 60 mL/min to carry the vapour. After adsorption at 323 K, the temperature was increased (373, 473 and 573 K) flowing He in order to desorb the organic molecule and spectra were recorded. Scan resolution was 4 cm^{-1} and 1024 scans were recorded at each point.

2.3. HDO of Model Molecules

The HDO of phenol in the vapor-phase was carried out in a fixed-bed flow reactor at atmospheric pressure of H_2 and 573 K. Diffusion limitations were ruled out based on the method of Madon and Boudart [45]. Catalyst particles (53-106 μm) were diluted with SiC particles (200-450 μm, mass ratio: SiC / catalyst = 3.0) to avoid localized heating. Prior to the reaction, the catalyst was reduced *in situ* under pure hydrogen (60 mL/min) at 573 K (10 K/min) for 1 h. The reactant mixture was obtained by flowing H_2 through the saturator containing phenol, which was kept at 347 K to obtain the desired H_2/phenol molar ratio 60 (0.0157 atm of phenol). To avoid condensation, all lines were heated to 523 K.

In one set of experiments, catalysts were tested at different W/F ratios, by varying catalyst amount (ranging from 5 to 25 mg) in order to obtain low conversion (around 10%). W/F is defined as catalyst mass (g) divided by mass flow rate (g/h) of the organic feed. Initial conversion was measured after 5 min to minimize the effect of catalyst deactivation. In another set of experiments, 60-150 mg of catalyst were used to obtain high conversion and to assess catalyst stability during 7 h of reaction. In a final experiment, the $Pd1Nb/SiO_2$ catalyst was first reduced under pure hydrogen (60 mL/min) at 773 K (10 K/min) for 1 h, and the feed was allowed to flow through the reactor until a significant drop in the phenol conversion took place. Then, catalyst

reactivation was performed by introducing a new reducing treatment (H_2 flow at 773 K for 1 h); finally, the reaction was carried out again. The reaction products were analyzed using an Agilent Technologies 7890A/5975C GCMS, equipped with a HP-Innowax capillary column and a flame-ionization detector (FID). The product yield and selectivity for each product were calculated as follows:

$$yield(\%) = \frac{mol\ of\ \ product\ produced}{mol\ of\ \ organic\ \ fed} \times 100 \quad (1)$$

$$Selectivity\ (\%) = \frac{mol\ of\ \ product\ produced}{mol\ of\ \ organic\ consumed} \times 100 \quad (2)$$

3. Results and Discussion

3.1. Catalyst Characterization

The BET surface areas of the catalysts are summarized in Table 1. All silica supported materials presented a quite similar specific surface area (150-170 m^2/g). The Pd/Nb_2O_5 catalyst exhibited a lower surface area (87 m^2/g).

The density of acid sites of the catalysts was measured by NH_3-TPD and by using the cyclohexanol dehydration reaction. The TPD profiles of desorbed ammonia are shown in Fig. 1. They exhibit multiple peaks poorly resolved between 300 and 800 K, indicating the presence of acid sites with different strength (weak: (T < 523 K); medium: (523 < T< 593 K); strong: (T > 593 K)). Furthermore, the intensity of the peaks increases with increasing Nb/Pd molar ratio. Table 1 reports the amount of desorbed ammonia and the acid strength distribution calculated from the NH_3-TPD profiles. The amount of desorbed ammonia on Pd/SiO_2 is very low, whereas Pd/Nb_2O_5 has the highest value (249 $\mu mol/g_{cat}$) that agree with the data reported in the literature [46]. The addition of niobia to Pd/SiO_2 catalyst led to the appearance of acidity to the catalysts. Increasing the Nb/Pd molar ratio increased the total amount of desorbed ammonia. However, the amount of desorbed ammonia for the sample with the highest niobia content ($Pd10Nb/SiO_2$) is still lower than that of Pd/Nb_2O_5. This result indicates that the silica support is not completely covered by Nb_2O_5 for the $Pd10Nb/SiO_2$ catalyst. The catalysts showed a similar acid strength distribution, indicating that the addition of niobia only increases the number of acid sites.

The cyclohexanol dehydration reaction has also been used to estimate the density of acid sites of the supports [30,41]. The dehydration of cyclohexanol to cyclohexene occurs on the acid sites of the support. Table 1 reports the reaction rate of dehydration of cyclohexanol (DHA) for the catalysts. The dehydration rate continuously

increases with the incorporation of niobia, which agrees very well with the NH_3-TPD results.

The electronic properties of the dispersed Nb_2O_5 phase on the PdNb/SiO_2 catalysts were investigated by UV-vis DRS spectroscopy. Because of the presence of an intense adsorption band of PdO, DRS spectra were obtained for a series of Nb_2O_5/SiO_2 materials without Pd, but with the same niobia loadings and prepared by the same procedure. The F(R) spectra (Fig. 2) showed an intense band corresponding to ligand-to-metal charge-transfer transitions (LMCT) from O^{2-} to Nb^{5+} in the domains of wavelengths of 200-400 nm. This band was shifted toward higher wavelength by increasing the niobia content. From the spectra in the UV-vis region, the band-gap energies were determined by the interception of the straight line fitted through the low energy side of the curve $(F(R).hv)^2$ versus hv, where F(R) is the Kubelka-Munk function and hv is the energy of the incident photon [47]. The corresponding band-gap energies are reported in Table 2. The band-gap energy is considered as the necessary energy to promote an electron transition from the valence band of the O 2p orbital to the conduction band of the Nb 4d orbital. In this work, the values of band-gap energies strongly depend on the Nb_2O_5 loading. For the amorphous Nb_2O_5, the band-gap energy is 3.76 eV, whereas this value is significantly higher for the silica supported catalysts containing lower niobia loading (4.05 – 4.25 eV). This indicates that a new type of niobia species was formed on the silica surface. Increasing the amount of niobia the band gap value decreases, approaching the value corresponding to that of amorphous bulk Nb_2O_5.

Surface niobia species are formed by the deposition of niobium precursors salts on high surface area oxide supports such as silica. Two different surface niobia species have been detected on oxide supports by various techniques (Raman, DRS, XANES),

depending on the surface coverage as well as the type of the support [48-51]. Four-fold coordinated surface NbO_4 species appear at low surface coverages, while six-fold coordinated surface NbO_6 species exist at high surface coverage. Each of these surface niobia species has different energy of absorption edge. Niobium oxide compounds with polymerized NbO_6 structure exhibit band-gap energies below 3.9 eV, while higher values are characteristic of isolated NbO_4 species [51,52]. Table 2 lists the band gap energies of some Nb-reference compounds and their corresponding structures. Gao et al. [51] found a band-gap energy of 4.37 eV for a 1%Nb_2O_5/SiO_2 and 3.97 eV for a 10% Nb_2O_5/SiO_2. These results were attributed to the presence of isolated NbO_4 species on the sample containing 1%Nb_2O_5, whereas the sample with high niobia content is represented by isolated NbO_4 as well as polymerized NbO_6 species. In the present work, the higher band-gap energy values obtained for the Pd0.5Nb/SiO_2, Pd1Nb/SiO_2 and Pd2.5Nb/SiO_2 catalysts could be attributed to isolated NbO_4 species dispersed on the silica. For the Pd10Nb/SiO_2 catalyst, the band gap values obtained could be assigned to polymerized NbO_6 species. The Pd5Nb/SiO_2 catalyst contained a mixture of isolated NbO_4 and polymerized NbO_6 species.

Figs.3 and 4 show the X-ray diffraction patterns recorded during *in situ* treatment of the Pd/SiO_2 and Pd5Nb/SiO_2 samples under He and 5% H_2/He mixture flow from 298 to 573. The diffractograms of the other catalysts are shown in Figs. S1 – S4. The diffractogram of Pd/SiO_2 at room temperature and He atmosphere exhibits a line at 2θ = 22.48° that is attributed to the PdO phase. When this sample is exposed to the H_2/He mixture at room temperature, the diffractogram remained unchanged. Increasing the temperature to 357 K, the line attributed to PdO disappears and a new line appeared at around 2θ = 26.5° that is attributed to the metallic Pd phase. For the PdNb/SiO_2 and Pd/Nb_2O_5 catalysts, the diffractograms of fresh samples (at room temperature and He

atmosphere) also exhibits the characteristic line of the PdO phase. However, when these samples are exposed to H_2 at room temperature, it is observed that the intensity of the line corresponding to the PdO phase decreases and a new line appears at $2\theta = 25.64^{o}$ that is likely due to the formation of the Pd hydride phase [53]. This result indicates that PdO is reduced to metallic Pd at room temperature, followed by the absorption of hydrogen into palladium, resulting in the formation of the Pd hydride phase. The increase in the temperature decreases the hydrogen solubility in Pd [54] and thus, heating the samples shifted this line to $2\theta = 26.46°$, indicating that Pd hydride was decomposed into metallic Pd. For the samples containing high niobia content ($Pd5Nb/SiO_2$ and $Pd10Nb/SiO_2$), the decomposition of Pd hydride to metallic Pd takes place at lower temperatures (331 and 327 K respectively). Furthermore, the formation/decomposition of Pd hydride phase is observed only on the catalysts containing niobia, suggesting an intimate contact between the niobia oxide species and the palladium, facilitating the palladium oxide reduction.

Table 3 lists the average crystallite size of Pd^0 obtained from the diffractograms after reduction of Pd-based catalysts at 573 K for 1h. Pd/SiO_2 and Pd/Nb_2O_5 catalysts have Pd^0 crystallite size of 6.7 and 4.5 nm, respectively. The addition of niobia to Pd/SiO_2 catalyst affected the crystallite size of metallic Pd. Increasing the Nb/Pd molar ratio to 1 slightly decreased the Pd^0 crystallite size to 4.5 nm. However, a significant growth of the crystallite size of metallic Pd was observed for the catalysts containing high niobia content (11.5 and 20.5 nm).

In situ XAS studies were performed to monitor the changes in catalyst structure during different treatments. Pd K-edge XANES spectra of Pd/SiO_2, Pd/Nb_2O_5 and $PdNb/SiO_2$ catalysts after reduction at 573 K are shown in Fig. 5. The spectra of all catalysts after reduction at 573 K are similar to that of the Pd foil, indicating that

palladium is fully reduced, regardless of the niobia content. Therefore, the chemical state of Pd after reduction at 573 K is not affected by the presence of niobia species.

Fig. S5 show the Inverse Fourier transform of the first peak at the Pd K-edge and experimental points as well as the k^3-weighed Fourier transformed spectra for the Pd/SiO_2, Pd/Nb_2O_5 and $PdNb/SiO_2$ catalysts after reduction at 573 K. Best fittings of Pd K-edge spectra obtained after cooling to 298 K under He are reported in Table S1. They revealed only the presence of Pd atoms in the first coordination shell of the absorber Pd atom. The addition of Pd-Nb scattering path into the fitting reduced the quality of the fit, indicating that Nb is not in the structure of Pd particles. Therefore, the local structure surrounding the Pd atoms does not change in the presence of Nb for these catalysts. Pd/SiO_2, $Pd1Nb/SiO_2$ and $Pd2.5Nb/SiO_2$ catalysts exhibit similar Pd-Pd average coordination number (N) (9.5 – 10.5 Å), which slightly increased for the samples containing higher niobia content (11.2 – 11.3 Å). The coordination number determined by EXAFS may give information about the Pd particle size [55]. In our work, an experimental relationship between the Pd particle size obtained by TEM/STEM and the Pd-Pd first shell coordination number (N) determined by EXAFS considering data from the literature [56-58] was used to estimate the Pd particle size (Table 3). The Pd particle size estimated using this methodology was 7.8 nm for Pd/SiO_2 and varied from 5.1 ($Pd1Nb/SiO_2$) to 11.6 nm ($Pd10Nb/SiO_2$) as the niobia content increased. It is noteworthy to see the agreement in the trends of Pd particle size calculated by EXAFS and XRD. Furthermore, the first coordination shell distances are also approximately the same for all supported Pd catalysts, regardless the niobia loading.

The XANES spectra at the Nb K-edge for $Pd1Nb/SiO_2$ and Pd/Nb_2O_5 catalysts (calcined and reduced at 573 K) are shown in Fig. 6. There is no significant change on

the spectra of the calcined and reduced catalysts. According to the literature, the reduction of Nb^{5+} to Nb^{4+} is reflected by a decrease in the intensity of pre-edge peak and it is also accompanied by a shift of the absorption edge to low energy [59-61]. In our work, the XANES spectra did not reveal the presence of partially reduced NbO_x species on $Pd1Nb/SiO_2$ and Pd/Nb_2O_5 catalysts after reduction at 573 K. This is not surprising, due to the low reduction temperature.

Figs. 7 and 8 show the TEM images and STEM-energy dispersive X-ray spectroscopy (EDS) elemental mappings of the reduced and passivated $Pd1Nb/SiO_2$ and $Pd10Nb/SiO_2$ catalysts, respectively. For the $Pd1Nb/SiO_2$ catalyst, the TEM image indicate that the Pd nanoparticles are well dispersed and uniformly distributed over the support with no significant agglomeration (Fig. 7A). In this case, the estimated Pd nanoparticle size distribution was centered between 3-4 nm as shown in the histogram (Fig. 7F). On the other hand, the TEM image for the $Pd10Nb/SiO_2$ catalyst (Fig. 8A) shows larger Pd nanoparticles and the formation of agglomerates on the support, resulting in a particle size distribution centered between 10-12 nm as depicted in Fig. 8F. Noticeably, no clear distinction between SiO_2 and Nb_2O_5 distribution are observed in the TEM images for both samples.

STEM-EDX analysis of $Pd1Nb/SiO_2$ (Figs. 7B-E) and $Pd10Nb/SiO_2$ (Figs. 8B-E) catalysts was used to investigate the elemental distribution. The elemental distribution for Si, Nb and Pd are depicted in blue, red and green. For the $Pd1Nb/SiO_2$ sample, the combined Si (blue), Nb (red) and Pd (green) maps (Fig. 7E) clearly confirm the presence of the three elements in the catalyst, in which Pd and Nb are very well dispersed on the support. However, there are regions on the surface of silica that are not covered by niobia, which is likely due to the low niobia content. Therefore, there are Pd particles deposited on silica as well as niobia. The STEM-EDX for the $Pd10Nb/SiO_2$

catalyst (Fig. 8D) clearly supports the formation of larger Pd nanoparticles and agglomerates. In spite of the agglomeration of Pd, the Nb elemental maps (Fig. 8C) indicate that niobia species are spread all over the surface of SiO_2, and thus most of the Pd particles are deposited over niobia (Fig. 8E), suggesting close contact between these elements. In fact, larger Pd particles are formed when they are located on niobia as revealed by TEM, XRD and EXAFS measurements.

3.2. HDO of Phenol

The HDO reaction of phenol was initially performed over pure SiO_2, 2% Nb_2O_5/SiO_2 and Nb_2O_5 supports. The supports did not show any measurable activity even at high W/F (0.53). These results indicate that the catalyst activity is attributed to the metallic function or the Pd-support interface.

The HDO reaction rate and product distribution at low phenol conversion (~ 10%) are reported in Table 4. While the Pd/SiO_2 catalyst exhibited the lowest HDO reaction rate, the addition of very low amounts of niobia (e.g., Nb/Pd = 0.5, $Pd0.5Nb/SiO_2$ catalyst) significantly increased the activity (8-folds). The $Pd1Nb/SiO_2$ catalyst shows the highest HDO reaction rate among the silica supported catalysts. Further increase in the niobium content significantly decreased the HDO reaction rate as well as the overall reaction rate, which could be correlated with a decrease in the Pd dispersion with increasing Nb content, as observed by the *in situ* XRD analysis and TEM images.

Regarding product distribution, the main products obtained are benzene and cyclohexanone, with small amounts of cyclohexanol, cyclohexane and biphenyl. Minor products such as biphenyl and cyclohexane are formed by acid-catalyzed reactions such as alkylation and dehydration, respectively. Biphenyl might be produced by alkylation

of the phenolic ring with cyclohexanone over acid sites [62] followed by deoxygenation. Cyclohexane can be produced by dehydration of cyclohexanol followed by hydrogenation to cyclohexane. The higher selectivity to cyclohexane is observed on the catalysts with no cyclohexanol formation, suggesting that this compound was completely dehydrated on the acid sites. The formation of cyclohexane by hydrogenation of benzene in our work was not considered since this reaction is thermodynamically unfavorable at 573 K [63]. Based on the equilibrium constants calculated by Griffin et al. [22] for the interconversion between 3-methyl-cyclohexane and toluene as a function of temperature, the formation of 3-methyl-cyclohexane is thermodynamically favored at temperatures lower than ~ 530 K while the aromatic compound is formed at higher temperatures such as 573 K. Biphenyl and cyclohexane are mainly formed on the PdNb/SiO_2 and Pd/Nb_2O_5 catalysts that exhibited higher acidity.

The product distribution was significantly dependent on the Nb content. For Pd/SiO_2, the main product formed is cyclohexanone but the addition of Nb_2O_5 significantly increases the selectivity to benzene. For the catalyst containing a very low amount of Nb (Nb/Pd molar ratio = 0.5), the selectivity to benzene is 8-fold higher than that of Pd/SiO_2. The selectivity to benzene increased up to a Nb/Pd molar ratio of 2.5 and then, it remained constant and similar to that of the Pd/Nb_2O_5 catalyst. This result suggests that the deoxygenation reaction is promoted by the niobia species. Furthermore, HDO of phenol reaction was carried out over a physical mixture of Pd/SiO_2 and Nb_2O_5 and the product distribution obtained was very similar to that observed for the Pd/SiO_2 catalyst, with high selectivity to cyclohexanone, regardless of the presence of Nb_2O_5. Therefore, intimate contact between Pd and Nb_2O_5 is required to

promote the deoxygenation reaction of phenol to benzene, indicating that the deoxygenation step takes place at the Pd-niobia interface.

3.3. The role of metal-support interfacial sites on deoxygenation activity

Fig. 9 reveals a remarkable increase in the benzene selectivity as a function of the Nb/Pd molar ratio. The benzene selectivity sharply increases from Pd/SiO_2 to $Pd1Nb/SiO_2$ catalyst and then it reaches a maximum at a Nb/Pd molar ratio of 2.5. Further increases in niobium content did not change the selectivity, suggesting that there is an optimum loading of niobia in the vicinity of Pd particles that is necessary to promote the deoxygenation reaction. In fact, the chemical mapping images for $Pd1Nb/SiO_2$ catalyst (Fig.7E) showed the presence of Pd particles over silica as well as close to the niobia species. The Pd particles deposited over the silica support should be responsible for the significant formation of cyclohexanone over this catalyst due to the absence of contact with niobia. For $Pd10Nb/SiO_2$ catalyst, the chemical mapping (Fig. 8E) images revealed that the majority of Pd particles are in close contact with niobia, leading to a high selectivity to benzene. Therefore, the results obtained suggest that the deoxygenation pathway occurs at the interface between metal sites and oxophilic sites (i.e., the Pd-Nb_2O_5 junction).

It is surprising that the addition of only 0.9 wt.% of niobia (Nb/Pd molar ratio = 0.5) leads to a selectivity to benzene of 24.7%. In order to obtain the degree of coverage of silica by niobia, cyclohexanol dehydration was used as a probe reaction. The dehydration rate increased linearly as a function of the Nb content, as shown in Fig. S6a. Taking into account that the acidity of silica is not significant and that the dehydration rate of Pd/Nb_2O_5 catalyst corresponds to complete coverage, a relationship

between the reaction rate of cyclohexanol dehydration and the degree of coverage of silica by niobia was established (Fig. S6b). For the silica supported catalyst with the highest amount of niobia (Pd10Nb/SiO_2), the degree of coverage was around 32%. Since the selectivity to benzene observed for this catalyst is similar to that of Pd/Nb_2O_5, the result shows that Pd is preferentially deposited over niobia, regardless of the low coverage degree of silica by Nb_2O_5.

This may be due to the co-impregnation method used. In this case, the palladium precursor in the solution is a cation, whereas the niobium oxalate is an anion. This difference in charge may favor the deposition of palladium precursor over niobium during the synthesis, leading to intimate contact between Pd particles and niobia after calcination.

The relationship between the deoxygenation activity and the Pd-Nb_2O_5 interface was also confirmed by carrying out the HDO of phenol reaction after reduction of Pd1Nb/SiO_2 and Pd10Nb/SiO_2 catalysts at different temperatures (Table 5). Increasing the reduction temperature from 573 to 773 K, the HDO reaction rate decreased for both catalysts. Regarding product distribution, changes were observed for the Pd1Nb/SiO_2 catalyst. The selectivity to benzene decreased while the formation of oxygenated products (cyclohexanone and cyclohexanol) increased. However, the product distribution remained unchanged when the reduction temperature increased for the Pd10Nb/SiO_2 catalyst.

The increase in reduction temperature may cause sintering of Pd as well as the coverage of Pd particles by partially reduced NbO_x species that are formed, since niobia is known as a reducible support [64,65]. In this work, *in situ* XRD during reduction until 773 K did not show significant growth of the Pd particles for the Pd1Nb/SiO_2 and Pd10Nb/SiO_2 catalysts. Thus, metal sintering may be ruled out (Table S2).

Therefore, the results indicate that the decrease in the HDO reaction rate for both catalysts could be due to the coverage of palladium particles by the NbO_x species after reduction at high temperature. However, this does not explain the change in product selectivity observed for the $Pd1Nb/SiO_2$ catalyst. In fact, the reduction treatment might also affect the dispersion of niobium species by sintering with increasing the reduction temperature. This will reduce the niobia surface area, leading to losses in contact between Nb_2O_5 and Pd particles. Thus, the loss in the Pd-NbO_x interface will favor the hydrogenation to cyclohexanone over the Pd sites.

For the $Pd10NbSiO_2$ catalyst, the reaction rate also decreases but the selectivity to benzene does not change when the reduction temperature is raised. In this case, the DRS result for this catalyst suggested the presence of polymerized NbO_6 species. Thus, the increase in the reduction temperature will not cause significant sintering of niobium species. Moreover, the Nb_2O_5 species are well dispersed over the support due to the high niobium loading, as shown in the chemical mapping (Figure 8E). Then, the Pd-Nb interface is preserved, maintaining a high selectivity to benzene. These results emphasize the crucial role of the metal-oxophilic site interface for deoxygenation toward benzene during HDO of phenol.

Therefore, the metal-support interfacial sites play key roles in the activity and selectivity of HDO of phenol. Several evidences for the intimate contact between Pd particles and Nb_2O_5 species were obtained by the different *in situ* characterization techniques used in our work: (i) the formation/decomposition of the Pd hydride phase that takes place only on the catalysts containing niobia, which facilitates the reduction of PdO; (ii) the Pd sintering when Pd particles are deposited over niobia, as revealed by TEM, XRD and EXAFS. On the other hand, XANES spectra showed that Pd is completely reduced for all $PdNb/SiO_2$ catalysts, indicating that niobia does not change

the chemical state of Pd. Furthermore, the first coordination shell and the Pd-Pd distances are not affected by the addition of niobia. Therefore, the Pd-Nb_2O_5 interaction consists of physical contact between Pd particles and niobia species that favors the sequential reaction steps involved in the HDO mechanism: (i) hydrogen adsorption and activation on Pd surface particles and; (ii) phenol adsorption on Nb_2O_5 species followed by hydrogenation of C=O bond with hydrogen spilt over from the metal sites.

However, we cannot rule out the influence of the structure of Nb_2O_5 species in the enhancement of benzene selectivity. UV-VIS diffuse reflectance spectroscopy was used to shed light on the structure of the Nb_2O_5 species on silica. The results indicated the formation of different structures of Nb_2O_5 species on the silica surface such as isolated NbO_4 species or polymerized NbO_6 species. Considering that the isolated NbO_4 species have a lower coordination number than NbO_6, these species may establish a stronger bond with the oxygen atom from phenol, thereby rapidly increasing the deoxygenation rate. This may be supported by the significant increase in benzene selectivity observed with addition of up to 4.6 wt% of niobium (Nb/Pd molar ratio = 2.5), in which the catalysts present only NbO_4 species. For the catalyst presenting polymerized NbO_6 species the benzene selectivity remained constant.

3.4. The effect of support on reaction mechanism

According to the reaction mechanism proposed for HDO reaction of phenol, three different reaction pathways can take place depending on the type of support or the nature of the metal-oxide interface: (i) hydrogenation of the aromatic ring and the formation of cyclohexanone and cyclohexanol followed by its dehydration; (ii) direct deoxygenation or (iii) hydrogenation of the carbonyl function of the keto tautomer intermediate which is rapidly converted to benzene via dehydration. The catalyst acidity

is decisive in promoting route (i), while oxophilicity promotes the formation of benzene via routes (ii) or (iii). The acid properties of niobium oxide are well known in the literature [66]. Since several studies about the HDO reaction propose that route (i) is the main HDO reaction pathway over catalysts with sufficient acidity, the increase in benzene selectivity in this work could be due to the increase in the acidity of the catalysts by increasing the niobium oxide content.

In our previous works, we did not observe any correlation between acidity and deoxygenation activity [30,31,67]. When the HDO of phenol reaction was carried out over a Pd/Nb_2O_5 catalyst reduced at two different temperatures (573 and 773 K), the products distribution remained constant, whereas the density of acid sites decreased with the reduction temperature. DRIFTS experiments of desorbed cyclohexanone revealed that the strength of the bond between the oxygen and Nb^{5+}/Nb^{4+} cations was similar, regardless of the reduction temperature. This result indicates that the oxophilicity of Nb^{4+} and Nb^{5+} cations are approximately the same, which leads to the same selectivity to benzene [31]. Recently, we studied the effect of the type of support (SiO_2, CeO_2, Al_2O_3, TiO_2, ZrO_2) on the performance of Pd-based catalysts for the HDO of phenol and found no correlation between the catalyst acidity and deoxygenation activity [30]. The Pd/Al_2O_3 catalyst exhibited similar product distribution as compared to the Pd/SiO_2 catalyst (11 and 8% selectivity to benzene respectively) despite a significant difference in acidity (339 versus 8 $\mu mol/g_{cat}$ of ammonia desorbed). Furthermore, the deoxygenation activity and oxophilicity measured by DRIFTS of adsorbed cyclohexanone experiments followed the same order: $Pd/TiO_2 > Pd/ZrO_2 > Pd/Al_2O_3 \approx Pd/CeO_2 \approx Pd/SiO_2 \approx Pd/CeZrO_2$. No direct correlation between the deoxygenation activity for HDO of phenol and the density of acid sites or the concentration of defects on the support was observed for a series of $Pd/Ce_xZr_{(1-x)}O_2$ (x =

0.00; 0.25; 0.50; 0.75; 0.90) catalysts . In this case, the selectivity to benzene was also correlated with the oxophilicity of the support given by the presence of Zr^{4+}/Zr^{3+} cations [67].

In order to investigate the role of the acid sites on the deoxygenation activity of $PdNb/SiO_2$ catalysts, the variation in benzene selectivity and the acidity estimated by the dehydration of cyclohexanol reaction was plotted as a function of niobium content (Fig. 9). It can be observed that the density of acid sites continuously increased with the Nb content, as expected. However, the benzene selectivity sharply increased and reached a maximum with a niobium content of just 4.6 wt %. Then, benzene selectivity remained constant while the acidity of the catalysts further increased, indicating that there is not a correlation between acidity and phenol deoxygenation.

In the present study, DRIFTS experiments of adsorbed phenol over Pd/Nb_2O_5 were carried out to shed light on the reaction mechanism taking place. The spectra obtained after desorption at different temperatures are shown in Fig. 10. After desorption at 323 K, the bands at 1257, 1492, 1588 and 3069 cm^{-1} correspond to the vibration modes of adsorbed phenoxy species, indicating that phenol is dissociatively adsorbed over metal oxide cation [20,30]. Increasing the temperature to 373 K decreases the intensities of the bands attributed to phenoxy species and a new band is now clearly seen at 1653 cm^{-1}. This band is assigned to the adsorbed 2,4-cyclohexadienone, the tautomer of phenol [20]. The presence of this band confirms that the tautomerization mechanism takes place for the HDO of phenol. According to the tautomerization mechanism (Scheme 1), the hydrogenation of the carbonyl group of this keto-tautomer intermediate produces a cyclohexadienol intermediate that is rapidly dehydrated to benzene. This reaction pathway is favored over oxophilic supports such as zirconia, titania and niobia. However, the strong interaction between the oxophilic support

represented by the Nb^{+5} cation and the oxygen atom from the adsorbed intermediate molecule could also reduce the energy barrier for the cleavage of the C-O bond, as has been suggested in the literature for titania supported catalysts (direct deoxygenation) [27].

3.5. Stability of PdNb/SiO_2 catalysts for HDO of Phenol

In order to investigate the stability of the catalysts, the HDO reaction was monitored during 7 h of reaction. Figs. 11 and S7-S12 show the conversion of phenol and product distribution as a function of time on stream (TOS). No deactivation was observed for Pd/SiO_2 catalyst. However, all catalysts containing niobium strongly deactivated during the reaction, but the degree of deactivation seems to be affected by the niobium content. Changes in the product distribution also occurred with TOS depending on the catalyst composition. For the Pd0.5Nb/SiO_2 catalyst, benzene selectivity decreases, and the formation of cyclohexanone significantly increases in the first 100 min of TOS. Then, the product selectivity remains unchanged, even with further decreases in phenol conversion. For the Pd1Nb/SiO_2 catalyst, a similar behavior is observed but the variation in benzene and cyclohexanone selectivity is less significant. For Pd5Nb/SiO_2, Pd10Nb/SiO_2 and Pd/Nb_2O_5 catalysts, the selectivity to benzene and cyclohexanone only slightly varied at the beginning of the reaction and then remained unchanged, in spite of the strong loss of activity.

As verified herein and previously proposed [30,31], the phenol HDO reaction requires a metal-oxophilic site interface in order to take place selectively. The oxophilic site is required to adsorb the oxy-compounds and to promote their oxygen removal. Therefore, the loss in activity as well as changes in the product distribution could be associated with the loss of that interface. This, in turn, could be associated with: (i)

carbon deposition; (ii) strong adsorption of phenolic intermediates on the surface and (iii) metal sintering, decreasing the metal-support interface and the number of exposed interfaces.

The formation of carbonaceous species during the reaction was investigated by TPO of the spent catalysts. The TPO profiles (Fig. 12) of the spent catalysts after HDO of phenol depended on the Nb/Pd molar ratio. Pd/SiO_2 and $PdNb/SiO_2$ catalysts with Nb/Pd molar ratio ≤ 1 exhibited a broad and intense peak centered at 853 K. Increasing the niobia content, one narrow peak at 453-500 K and a broad peak between 523-673 K start to appear and their intensities increase as a function of niobium content. These different peaks can be due to various types of carbon or to different location of the carbon on the catalyst surface [68]. The intense peak centered at 853 K was not observed on the Pd/Nb_2O_5 catalyst, indicating the deposition of this type of carbon only on the silica support. However, no deactivation was observed for Pd/SiO_2 catalyst, suggesting that this type of carbon may not be formed on the metal surface and then, it is not responsible for the loss of catalyst activity. On the other hand, deactivation started to occur and increases as a function of the Nb/Pd molar ratio, which in turn is accompanied by increases in the intensity of the peak at low temperature. However, the temperature of the first oxidation region is low compared to the usual temperature reported for oxidation of carbon deposits. A similar experiment was previously performed by our group and it was shown that these peaks observed at low temperatures (453-673 K) are associated with the oxidation of strongly adsorbed intermediate species at the catalyst surface [32]. This strong interaction may contribute to the accumulation of oxygenated intermediates on the Pd-NbO_x interface, thus leading to catalyst deactivation.

Since the catalysts with low content of niobium significantly deactivated even showing very small peaks at low oxidation temperature, metal sintering was investigated as another possible cause of catalyst deactivation. To this end, Pd1Nb/SiO_2 catalyst was first reduced at 773 K and the reaction was carried out until a significant drop in the conversion took place (Fig. S13). After the removal of the adsorbed compounds with pure H_2 flow at 773 K, the reaction was re-started but the phenol conversion was not recovered. In fact, the phenol conversion continued to drop, indicating the occurrence of metallic sintering during the reaction, which also contributed to catalyst deactivation.

4. Conclusions

This work attempted the design of interfacial sites between Pd metal particles and Nb_2O_5 species dispersed over a silica support to catalyze the hydrodeoxygenation of phenol in the gas phase.

The addition of niobium significantly affected the activity and products distribution. Cyclohexanone was the main product formed over Pd/SiO_2 while benzene formation is promoted with the addition of niobium oxide. Comparing the variation in selectivity to benzene with the continuous addition of niobium, it is clear that niobia species promote benzene formation, thus demonstrating the interplay of the metal-support interface in controlling reaction pathways towards the deoxygenation of phenol. The product distribution agrees with the reaction mechanism based on the tautomerization of phenol which was confirmed by DRIFTS experiments. We have found that Pd particles supported on silica favor ring hydrogenation of the

cyclohexadienone tautomer while the Pd particles in contact with Nb_2O_5 species enables the selective hydrogenation of the C=O bond to occur, producing benzene. No direct relationship was observed between deoxygenation activity and the acidity of the catalysts; rather, the formation of deoxygenation products depended on the contact between Nb^{5+} oxophilic cations and the metal particles. These results provide novel insights into the control of selectivity in the HDO reaction and indicate that the rational combination of hydrogenation and oxophilic properties in a Pd-Nb_2O_5 interface create the active sites responsible for deoxygenation and thus, a promising system for bio-oil upgrading.

Acknowledgments

The authors thanks CAPES (Finance code 001), FAPERJ (E-26/202.783/2017) and CNPq (303667/2018-4; 305046/2015-2; 302469/2020-6) for scholarship and financial support. Thanks for the LNLS for the assigned beamtime at XRD-1 (20180264) to perform the XRD studies and XDS (20180262, 20170409) for the XAS experiments. Support from the National Science Foundation (EPSCoR0814361), US Department of Energy (DE-FG36GO88064), Oklahoma Secretary of Energy and the Oklahoma Bioenergy Center are greatly appreciated.

REFERENCES

[1] E. Furimsky, App. Catal A. 199 (2000) 147-190.

[2] E.-J. Shin, M.A. Keane, Ind. Eng. Chem. Prod. Res. 39 (2000) 883-892.

[3] E. Díaz, A.F. Mohedano, L. Calvo, M.A. Gilarranz, J.A. Casas, J.J. Rodríguez, Chem Eng. J. 131 (2007) 65-71.

[4] A.J. Foster, P.T.M. Do, R.F. Lobo, Top. Catal. 55 (2012) 118-128.

[5] H. Wan, R.V. Chaudhari, B. Subramaniam, Top. Catal. 55 (2012) 129-139.

[6] W. Song, Y. Liu, E. Baráth, C. Zhao, J.H. Lercher, Green Chem. 17 (2015) 1204-1218.

[7] D. Gao, C. Schweitzer, H.T. Hwang, A. Varma, Ind. Eng. Chem. Res. 53 (2014) 18658-18667.

[8] Y. Hong, H. Zhang, J. Sun, K.M. Ayman, A.J.R. Hensley, M. Gu, M.H. Engelhard, J-S. McEwen, Y. Wang, ACS Catal. 4 (2014) 3335-3345.

[9] A.J.R. Hensley, Y. Wang, J-S. McEwen, ACS Catal. 5 (2015) 523-536.

[10] M. Saidi, F. Samimi, D. Karimipourfard, T. Nimmanwudipong, B.C. Gates, M.R. Rahimpour, Energy Environ. 7 (2014) 103-129.

[11] Y. Romero, F. Richard, S. Brunet, App. Catal. B 98 (2010) 213-233.

[12] M.J. Mendes, O.A.A. Santos, E. Jordao, A.M. Silva, App. Catal. A 217 (2001) 253-262.

[13] K. Kreuzer, R. Kramer, J. Catal. 167 (1997) 391-399.

[14] C. Newman, X. Zhou, B. Goundie, I.T. Ghampson, R.A. Pollock, Z. Ross, M.C. Wheeler, R.W. Meulenberg, R.N. Austin, B.G. Frederick, App. Catal. A: Gen. 477 (2014) 64-74.

[15] Q. Tan, G. Wang, L. Nie, A. Dinse, C. Buda, J. Shabaker, D.E. Resasco, ACS Catal. 5 (2015) 6271-6283.

[16] M. Shetty, K. Murugappan, T. Prasomsri, W.H. Green, Y. Róman-Leshkov, J. Catal. 331 (2015) 86-97.

[17] X. Zhu, L. Nie, L.L. Lobban, R.G. Mallinson, D.E. Resasco, Energy Fuels 28 (2014) 4104-4111.

[18] L. Nie, D.E. Resasco, J. Catal. 317 (2014) 22-29.

[19] L. Nie, P.M. De-Souza, F.B. Noronha, W. An, T. Sooknoi, D.E. Resasco, J. Mol. Catal. A Chem.388-389 (2014) 47-55.

[20] P.M. De-Souza, R.C. Rabelo-Neto, L.E.P. Borges, G. Jacobs, B.H. Davis, T. Sooknoi, D.E. Resasco, F.B. Noronha, ACS Catal. 5 (2015) 1318-1329.

[21] C.A. Teles, R.C. Rabelo-Neto, J.R. Lima, L.V. Mattos, D.E. Resasco, F.B. Noronha, Catal. Let. 146 (2016) 1848-1857.

[22] M.B. Griffin, G.A. Ferguson, D.A. Ruddy, M.J. Biddy, G.T. Beckham, J.A. Schaidle, ACS Catal. 6 (2016) 2715-2727.

[23] A.M. Robinson, G.A. Ferguson, J.R. Gallagher, S. Cheah, G.T. Beckham, J.A. Schaidle, J.E. Hensley, J.W. Medlin, ACS Catal. 6 (2016) 4356-4368.

[24] I.T. Ghampson, C. Sepúlveda, A.D. Dongil, G. Pecchi, R. García, J.L.G. Fierro, N. Escalona, Catal. Sci. & Technol. 6 (2016) 7289-7306.

[25] T.O. Omotoso, B. Baek, L.C. Grabow, S.P. Crossley, ChemCatChem 9 (2017) 2642-2651.

[26] H-Y. Chen, G. Pacchioni, ChemCatChem 8 (2016) 2492-2499.

[27] R.C. Nelson, B. Baek, P. Ruiz, B. Goundie, A. Brooks, M.C. Wheeler, B.G. Frederick, L.C. Grabow, R.N. Austin, ACS Catal. 5 (2015) 6509-6523.

[28] S.M. Schimming, O.D. LaMont, M. Konig, A.K. Rogers, A.D. D'Amico, M.M. Yung, C. Sievers, ChemSusChem 8 (2015) 2073-2083.

[29] W. Wang, K. Wu, P. Liu, L. Li, Y. Yang, Y. Wang, Ind. Eng. Chem. Res. 55 (2016) 7598-7603.

[30] P.M. De-Souza, R.C. Rabelo-Neto, L.E.P. Borges, G. Jacobs, B.H. Davis, D.E. Resasco, F.B. Noronha, ACS Catal. 7 (2017) 2058-2073.

[31] A.M. Barrios, C.A. Teles, P.M. De-Souza, R.C. Rabelo-Neto, G. Jacobs, B.H. Davis, F.B. Noronha, Catal. Today 302 (2018) 115-124.

[32] C.A. Teles, P.M. De-Souza, R.C. Rabelo-Neto, M.B. Griffin, C. Mukarakate, K. A. Orton, D.E. Resasco, F.B. Noronha, App. Catal. B 238 (2018) 38-50.

[33] K.A. Resende, A.H. Braga, F.B. Noronha, C.E. Hori, App. Catal. B 245 (2019) 100-113.

[34] P. Sirous-Rezaei, J. Jae, K. Cho, C.H. Ko, S-C. Jung, Y-K. Park, Chem. Eng. J. 377 (2019) 120121.

[35] N.N. Duong, D. Aruho, B. Wang, D.E. Resasco, Chinese J. Catal. 40 (2019) 1721-1730.

[36] L. Kong, L. Zhang, J. Gu, L. Xie, Y. Wang, L. Dai, Bioresour. Technol. 299 (2020) 122582.

[37] J. Zhang, J. Sun, B. Sudduth, X.P. Hernandez, Y. Wang, Catal. Today, 339 (2020) 305-311.

[38] J. Xi, Q. Xia, Y. Shao, D. Ding, P. Yang, X. Liu, G. Lu, Y. Wang, App. Catal. B 181(2016) 699-706.

[39] Q-N. Xia, Q. Cuan, X-H. Liu, X-G. Gong, G-Z. Lu, Y-Q. Wang, Angew. Chem. Int. Ed. 53 (2014) 9755-9760.

[40] J. Zhang, B. Wang, E. Nikolla, J.W. Medlin, Angew. Chem. Int. Ed. 56 (2017) 1-6.

[41] D. Martin, D. Duprez. J. Mol. Catal. A: Chem. 118 (1997) 113-128.

[42] A.M.G. Carvalho, D.H.C. Araújo, H.F. Canova, C.B. Rodella, S.L. Cuffini, R.N. Costa, R.S. Nunes, J. Synchrotron Radiat. 23 (2016) 1501-1506.

[43] F.A. Lima, M.E. Saleta, R.J. Pagliuca, M.A. Eleotério, R.D. Reis, J. Fonseca-Júnior, B. Meyer, E.M. Bittar, N.M. Souza-Neto, E. Granado, Journal of Synchrotron Rad. 23 (2016) 1538-1549.

[44] B. Ravel, M. Newville, J. Synchrotron Rad. 12 (2005) 537-541.

[45] R.J. Madon, M. Boudart, Ind. & Eng. Chem. Fund. (1982) 438-447.

[46] H.N. Pham, Y.J. Pagan-Torres, J.C. Serrano-Luiz, D. Wang, J.A. Dumesic, A.K. Datye. App. Catal. A: Gen. 397 (2011) 153-162.

[47] R.S.G. Ferreira, P.G.P. De Oliveira, F.B. Noronha. App. Catal. B 29 (2001) 275-283.

[48] I.E. Wachs, J.M. Jehng, G. Deo, H. Hu, N. Arora, Catal. Today 28 (1996) 199-205.

[49] I.E. Wachs, L.E; Briand, J-M. Jehng, L. Burcham, X. Gao, Catal. Today 57 (2000) 323–330.

[50] J. He, Q-J. Li, Y-N. Fan, J. Solid State Chem. 202 (2013) 121–127.

[51] X. Gao, I.E. Wachs, M.S. Wong, J.Y. Ying, J. Catal. 203 (2001) 18-24.

[52] J.M. Jehng, I.E. Wachs, Chem. Mater. 3 (1991) 100-107.

[53] F.A. Lewis, Academic press, London-New York, 1967.

[54] F.B. Noronha, M. Schmal, M. Primet, R. Frety, App. Catal. 78 (1991) 125-139.

[55] B.J. Kip, F.B.M. Duivenvoorden, D.C. Koningsberger, R. Prins, J. Catal. 105 (1987) 26-38.

[56] M.W. Tew, J.T. Miller, J.A.V. Bokhoven, J. Phys. Chem. C 113 (2009) 15140-15147.

[57] S. Sheu, J-F. Lee, S-G. Shyu, W-W. Chou, J-R. Chang, J. Catal. 266 (2009) 15-25.

[58] S. Hokenek, J.N. Kuhn, ACS Catal. 2 (2012) 1013-1019.

[59] Q. Jia, S. Ghoshal, J. Li, W. Liang, G. Meng, H. Che, S. Zhang, Z-F. Ma, S. Mukerjee, J. Am. Chem. Soc. 139 (2017) 7893-7903.

[60] S. Ghoshal, Q. Jia, M.K. Bates, J. Li, C. Xu, K. Gath, J. Yang, J. Waldecker, H. Che, W. Liang, G. Meng, Z-F. Ma, S. Mukerjee. ACS Catal. 7 (2017) 4936–4946

[61] R. Kodama, Y. Terada, I. Nakai, S. Komaba, N. Kumagai, J. Electrochem. Soc. 153 (2006) A583-A588.

[62] T. Nimmawudipong, R.C. Runnebaum, K. Tay, D.E. Block, B.C. Gates, Catal. Let. 141(2011) 1072-1078.

[63] C. Zhao, S. Kasakov, J. He, J.A. Lercher, J. Catal. 296 (2012) 12-23.

[64] Z. Hu, H. Nakamura, K. Kunimore, H. Asano, T. Uchijima, J. Catal. 112 (1988) 478-488.

[65] F.B. Noronha, B. Moraweck, P. Delichere, M. Brun, F. Villain, R. Frety, J. Phys. Chem. B 104 (2000) 5478-5485.

[66] M. Ziolek, Catal. Today 78 (2003) 47-64.

[67] C.A. Teles, P.M. De-Souza, A.H. Braga, R.C. Rabelo-Neto, A. Teran, G. Jacobs, D.E. Resasco, F.B. Noronha, App. Catal. B 249 (2019) 292-305.

[68] F.B. Noronha, E.C. Fendley, R.R. Soares, W.E. Alvarez, D.E. Resasco, Chem. Eng. J. 82 (2001) 21-31.

Figure captions

Figure 1. NH_3-TPD profiles of the catalysts.

Figure 2. (a) UV-vis DRS spectra and (b) determination of the position of the absorption edge of the Nb_2O_5/SiO_2 samples containing different niobium content.

Figure 3. Diffractograms of Pd/SiO_2 catalyst obtained during reduction under a 5%H_2/He mixture at different temperatures and XRD patterns at selected reduction temperatures: (a) He 298 K (b) H_2 298 K, (c) H_2 357 K and (d) H_2 573 K (♦) PdO; (•) Pd^0.

Figure 4. Diffractograms of $Pd5Nb/SiO_2$ catalyst obtained during reduction under a 5%H_2/He mixture at different temperatures and XRD patterns at selected reduction temperatures: (a) He 298 K (b) H_2 298 K, (c) H_2 331 K, (d) H_2 573 K. (♦) PdO; (♣) PdH; (•) Pd^0.

Figure 5. XANES spectra of after catalyst reduction in H_2/He at 573 K (measures taken at 293 in He): (a) Pd/SiO_2; (b) $Pd1Nb/SiO_2$; (c) $Pd2.5Nb/SiO_2$; (d) $Pd5Nb/SiO_2$; (e) $Pd10Nb/SiO_2$; (f) Pd/Nb_2O_5; (g) Pd foil.

Figure 6. The XANES spectra at the Nb K-edge for $Pd1Nb/SiO_2$ and Pd/Nb_2O_5 catalysts calcined and reduced at 573 K.

Figure 7. (A) TEM image; (B–E) STEM analysis and (F) respective Pd size distribution histogram for $Pd1Nb/SiO_2$ catalyst. (A) TEM bright field image in which the darkest contrast from Pd nanoparticles results from its higher atomic number as $Z_{Pd} > Z_{Nb} > Z_{Si}$. Corresponding EDS elemental maps of (B) Si, (C) Nb, and (D) Pd. (E) Corresponding EDS composite elemental map image.

Figure 8. (A) TEM image; (B–E) STEM analysis and (F) respective Pd size distribution histogram for $Pd10Nb/SiO_2$ catalyst. (A) TEM bright field image in which the darkest contrast from Pd nanoparticles results from its higher atomic number as $Z_{Pd} > Z_{Nb} > Z_{Si}$.

Corresponding EDS elemental maps of (B) Si, (C) Nb, and (D) Pd. (E) Corresponding EDS composite elemental map image.

Figure 9. Selectivity to benzene and rate of cyclohexanol dehydration reaction (DHA) as a function of the Nb/Pd molar ratio.

Figure 10. DRIFTS Spectra of TPD of phenol over the Pd/Nb_2O_5 catalyst.

Figure 11. Conversion of phenol as a function of TOS for the Pd/SiO_2, $PdNb/SiO_2$ and Pd/Nb_2O_5 catalysts. $T_{reduction}$: 573 K; $T_{reaction}$: 573 K, 1 atm.

Figure 12. TPO profiles of the spent catalysts after HDO reaction of phenol.

Scheme 1. Reaction routes for HDO of phenol over the supported Pd catalysts.

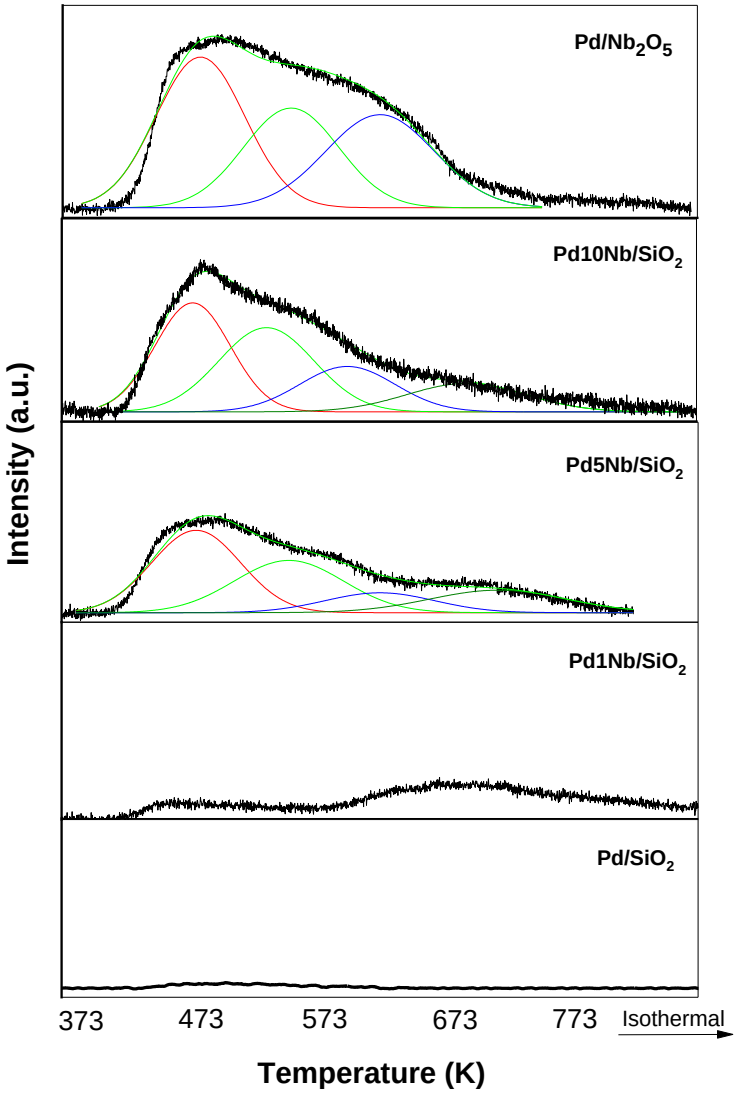

Figure 1. NH_3-TPD profiles of the catalysts.

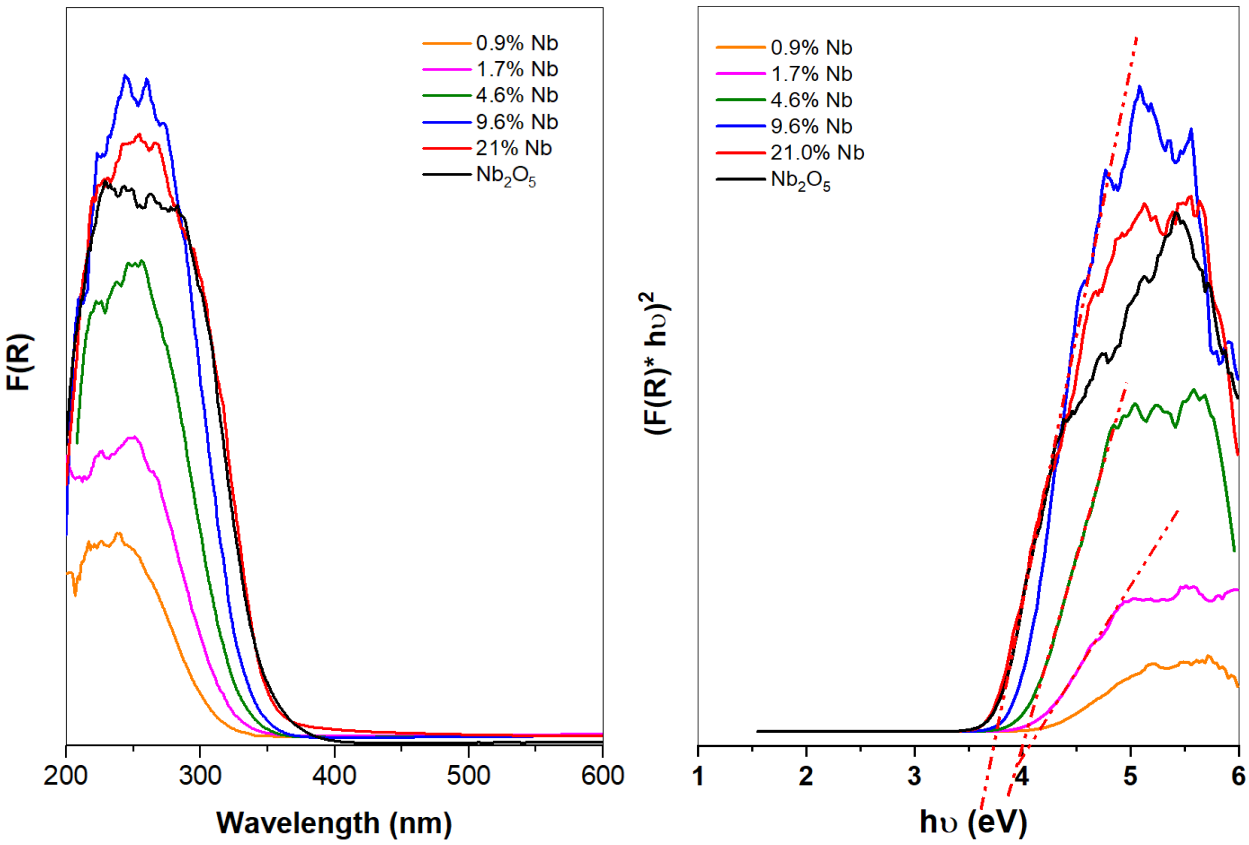

(a) (b)

Figure 2. (a) UV-vis DRS spectra and (b) determination of the position of the absorption edge of the Nb_2O_5/SiO_2 samples containing different niobium content.

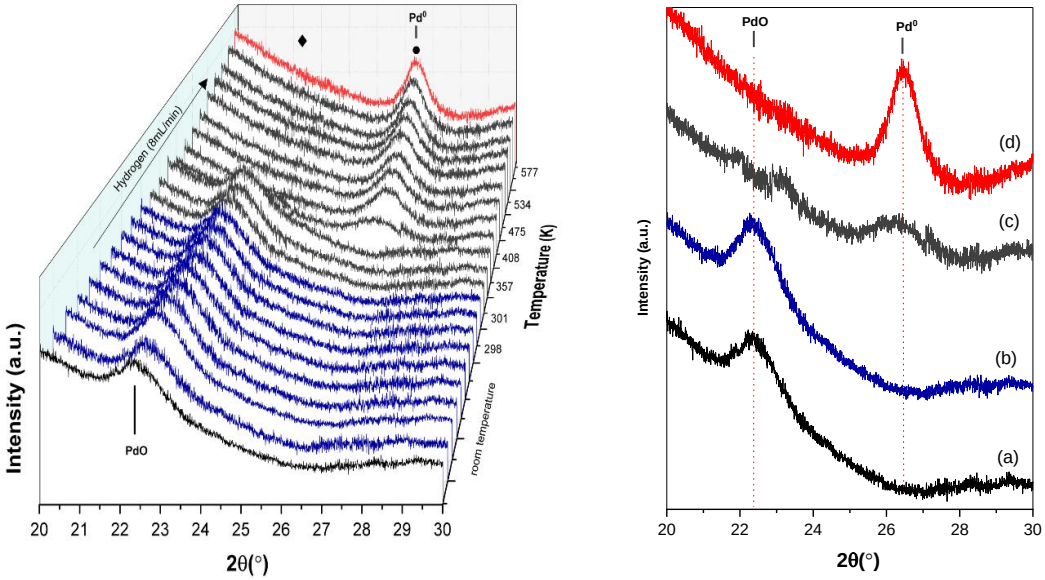

Figure 3. Diffractograms of Pd/SiO_2 catalyst obtained during reduction under a $5\%H_2/He$ mixture at different temperatures and XRD patterns at selected reduction temperatures: (a) He 298 K (b) H_2 298 K, (c) H_2 357 K and (d) H_2 573 K (♦) PdO; (●) Pd^0.

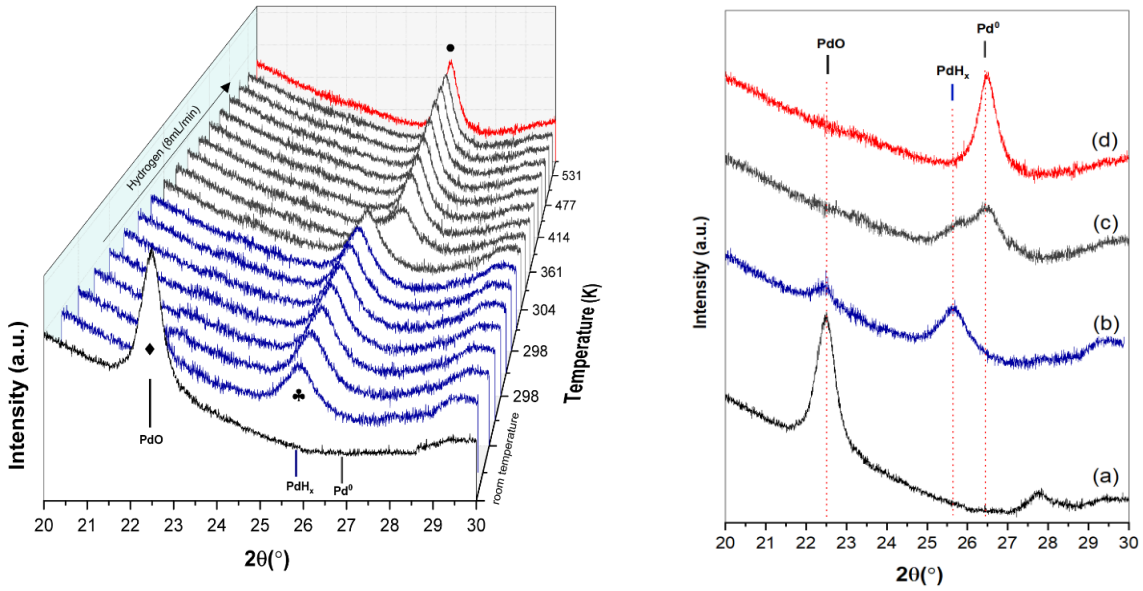

Figure 4. Diffractograms of Pd5Nb/SiO_2 catalyst obtained during reduction under a 5%H_2/He mixture at different temperatures and XRD patterns at selected reduction temperatures: (a) He 298 K (b) H_2 298 K, (c) H_2 331 K, (d) H_2 573 K. (♦) PdO; (♣) PdH; (●) Pd^0.

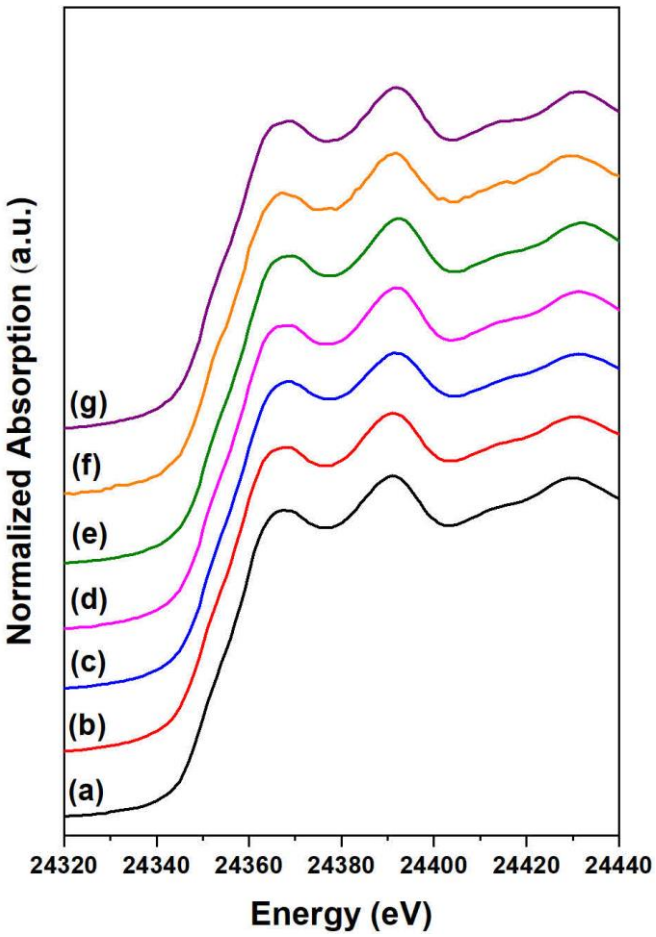

Figure 5. XANES spectra after catalyst reduction in H_2/He at 573 K (measures taken at 293 in He): (a) Pd/SiO_2; (b) Pd1Nb/SiO_2; (c) Pd2.5Nb/SiO_2; (d) Pd5Nb/SiO_2; (e) Pd10Nb/SiO_2; (f) Pd/Nb_2O_5; (g) Pd foil.

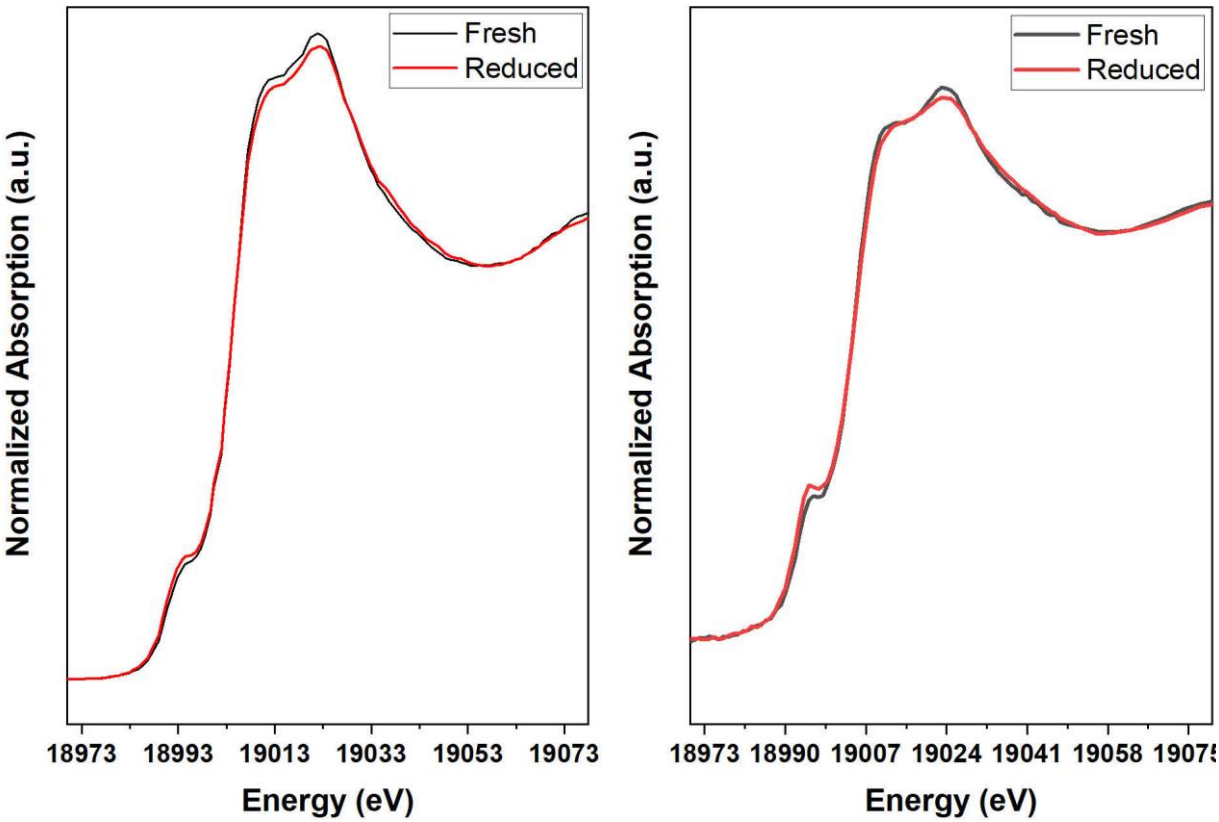

Figure 6. The XANES spectra at the Nb K-edge for (a) Pd/Nb_2O_5 and (b) $Pd1Nb/SiO_2$ catalysts calcined and reduced at 573 K.

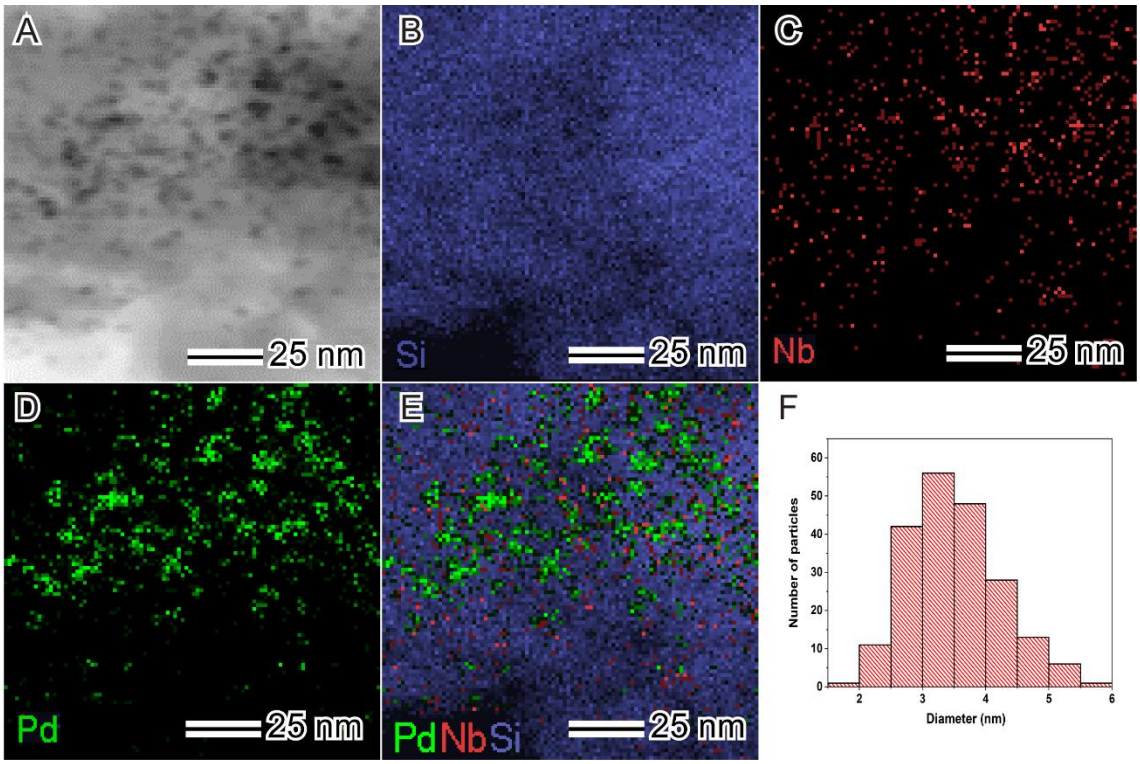

Figure 7. (A) TEM image; (B−E) STEM analysis and (F) respective Pd size distribution histogram for Pd1Nb/SiO_2 catalyst. (A) STEM brigh field image in which the darkest contrast from Pd nanoparticles results from its higher atomic number as $Z_{Pd} > Z_{Nb} > Z_{Si}$. Corresponding EDS elemental maps of (B) Si, (C) Nb, and (D) Pd. (F) Corresponding EDS composite elemental map image.

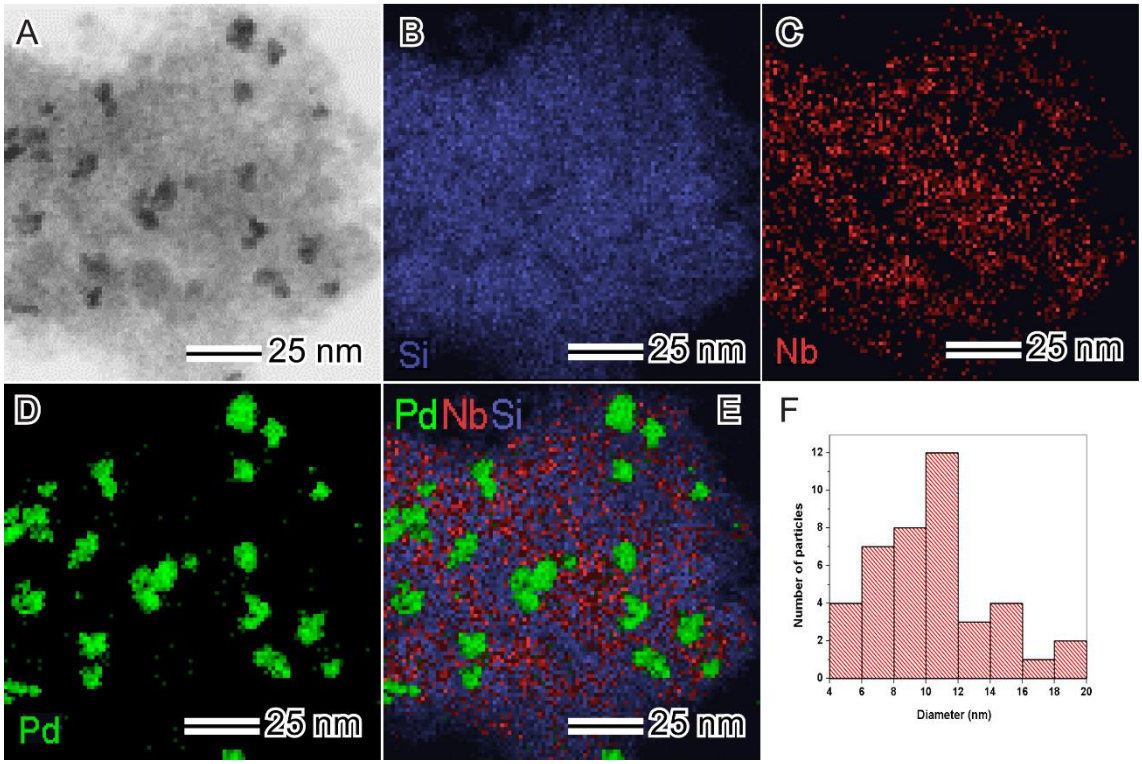

Figure 8. (A) TEM image; (B−E) STEM analysis and (F) respective Pd size distribution histogram for Pd10Nb/SiO_2 catalyst. (A) STEM brigh field image in which the darkest contrast from Pd nanoparticles results from its higher atomic number as $Z_{Pd} > Z_{Nb} > Z_{Si}$. Corresponding EDS elemental maps of (B) Si, (C) Nb, and (D) Pd. (F) Corresponding EDS composite elemental map image.

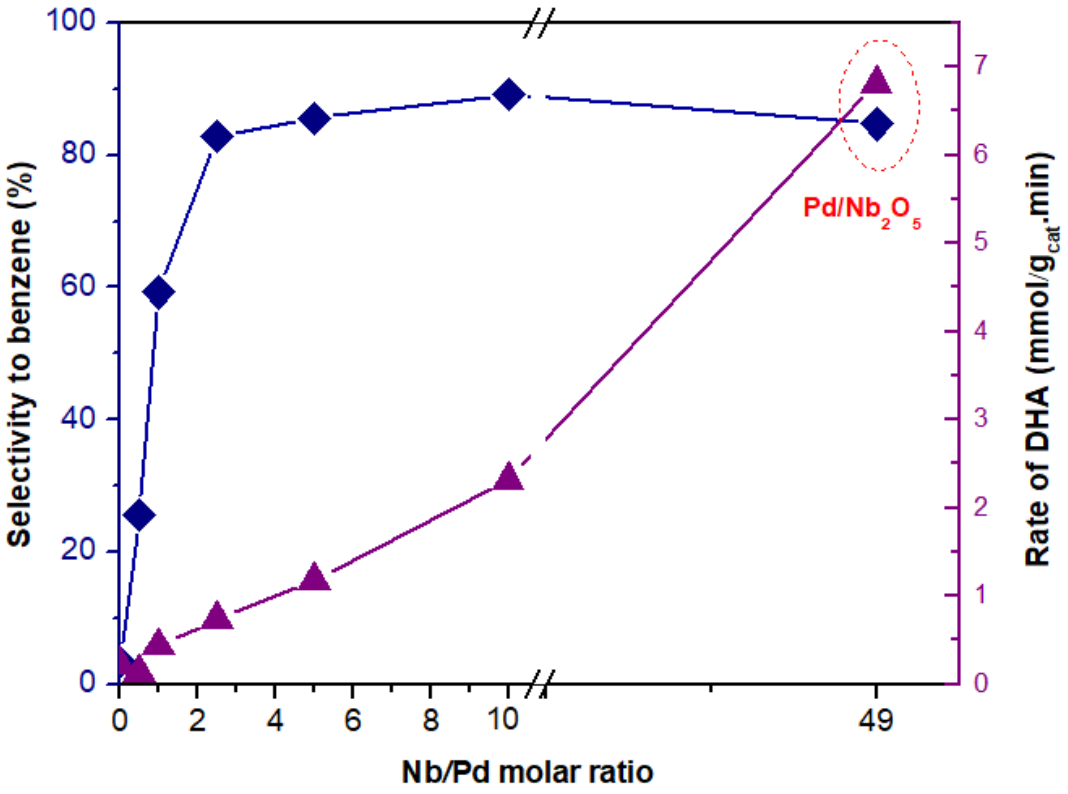

Figure 9. Selectivity to benzene and rate of cyclohexanol dehydration reaction (DHA) as a function of the Nb/Pd molar ratio.

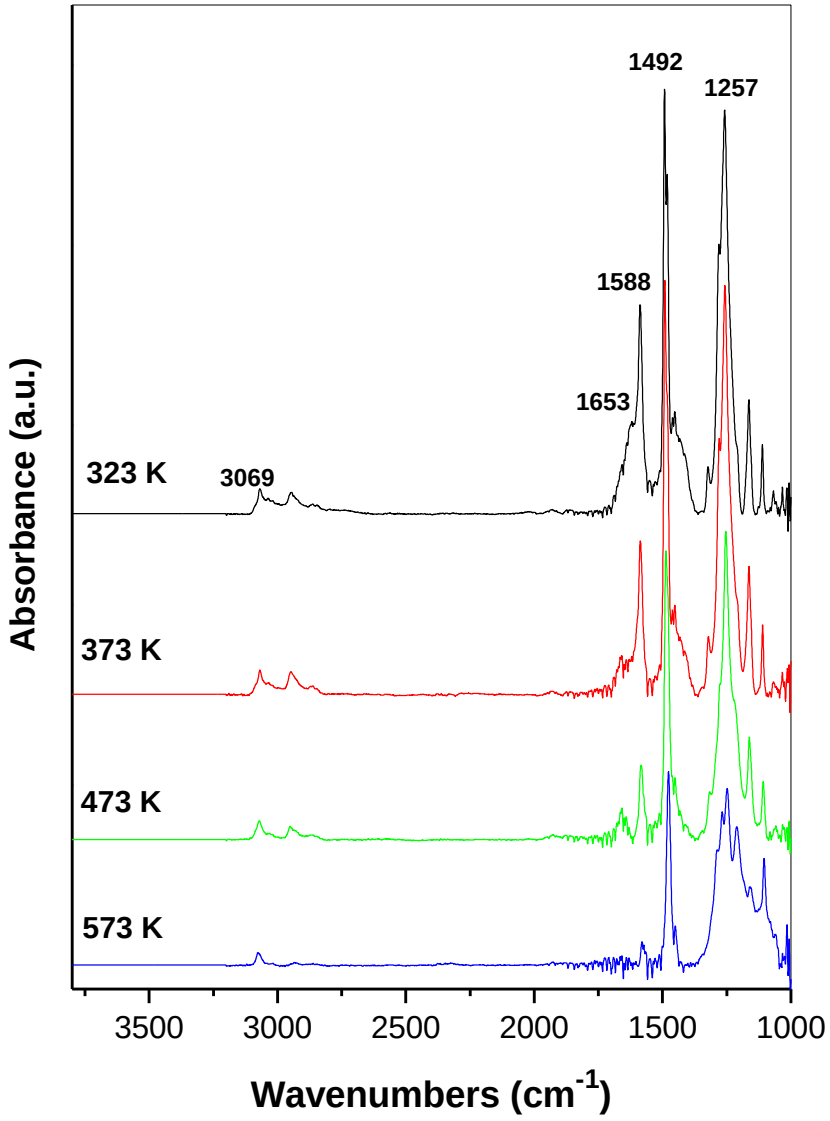

Figure 10. DRIFTS Spectra of TPD of phenol over the Pd/Nb_2O_5 catalyst.

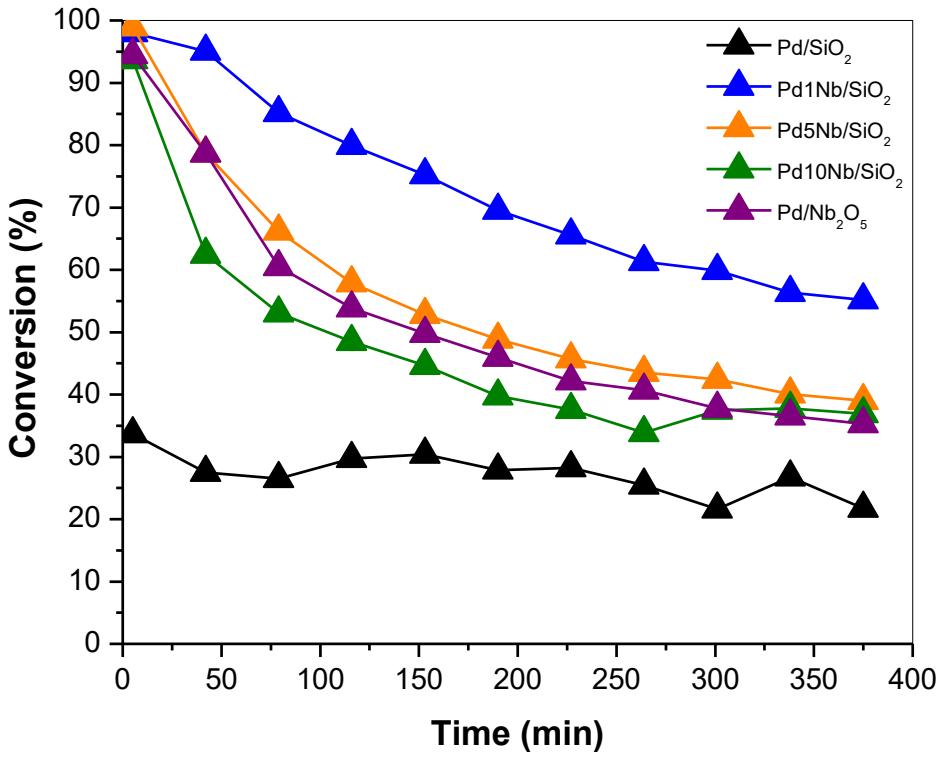

Figure 11. Conversion of phenol and product selectivity as a function of TOS for the Pd/Nb_2O_5 catalyst. $T_{reduction}$: 573 K; $T_{reaction}$: 573 K, 1 atm.

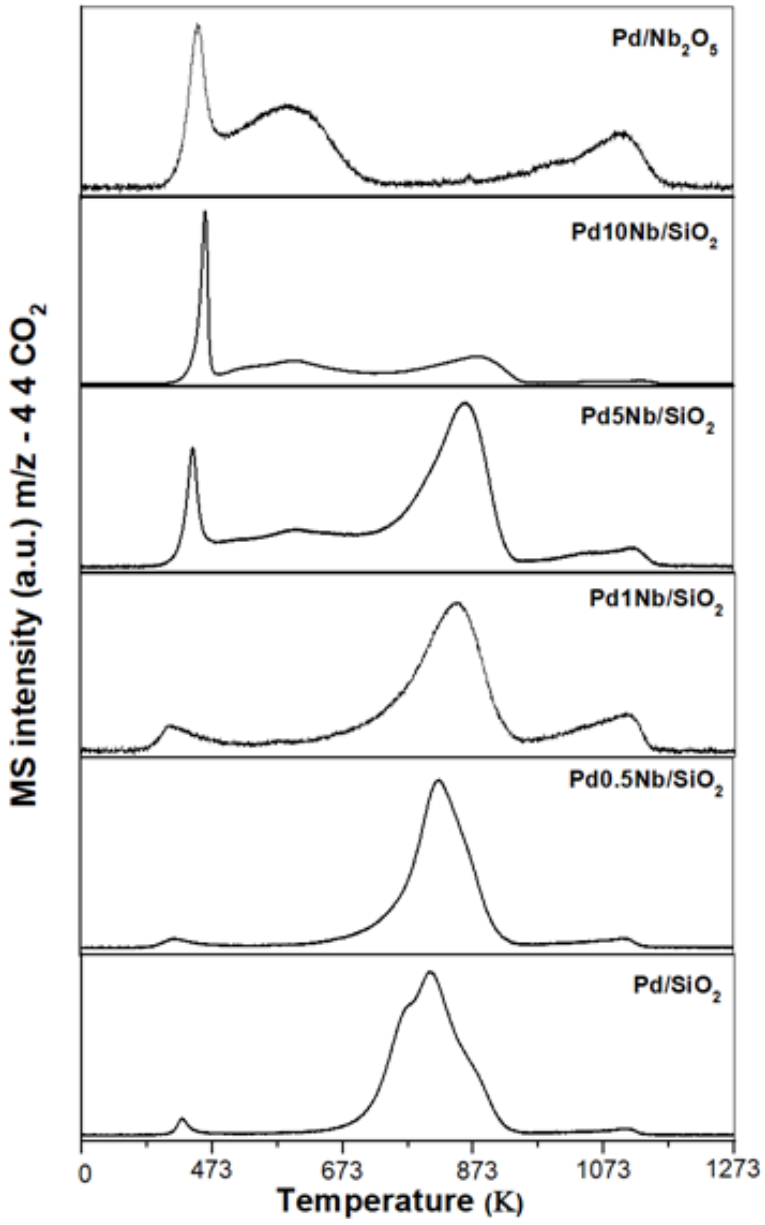

Figure 12. TPO profiles of the spent catalysts after HDO reaction of phenol.

Table 1. BET area, total amount of ammonia desorbed and respective acid strength distribution and cyclohexanol dehydration reaction rate of the catalysts.

Catalyst	BET (m^2/g)	Ammonia desorbed ($\mu mol/g_{cat}$)	Ammonia desorbed ($\mu mol/m^2$)	Acid sites distribution (%)			DHA rate ($mmol/g_{cat}.min$)
				Weak	Medium	Strong	
Pd/SiO_2	153	8	0.02	--	--	--	0.23
$Pd0.5Nb/SiO_2$	170	--	--	--	--	--	0.14
$Pd1Nb/SiO_2$	156	23	0.06	--	--	--	0.44
$Pd2.5Nb/SiO_2$	--	--	--	--	--	--	0.74
$Pd5Nb/SiO_2$	150	97	0.25	40	31	29	1.18
$Pd10Nb/SiO_2$	153	146	0.37	34	33	32	2.32
Pd/Nb_2O_5	87	249	1.12	38	34	27	6.82

Table 2. Band-gap energies of the containing-niobia catalysts.

Catalyst	Band gap energy (eV)	Structural assignment	Reference
$Pd0.5Nb/SiO_2$	4.25	Isolated NbO_4	This work
$Pd1Nb/SiO_2$	4.16	Isolated NbO_4	
$Pd2.5Nb/SiO_2$	4.05	Isolated NbO_4	
$Pd5Nb/SiO_2$	3.96	Isolated NbO_4+Polymerized NbO_6	
$Pd10Nb/SiO_2$	3.73	Polymerized NbO_x	
Nb_2O_5	3.76	Polymerized NbO_x	
$LiNbO_3$	3.89	Polymerized NbO_6	[51,52]
$NaNbO_3$	3.51	Polymerized NbO_6	
Nb_2O_5	3.42	Polymerized NbO_6	
$1\%Nb_2O_5/SiO_2$	4.37	Isolated NbO_4	
$10\%Nb_2O_5/SiO_2$	3.97	Isolated NbO_4+Polymerized NbO_6	
Nb-MCM41	4.43	Isolated NbO_4	

Table 3. Crystallite size of Pd^0 and Pd dispersion of the catalysts reduced at 573 K.

Catalyst	d_{Pd} (nm)[a]	d_{Pd} (nm)[b]	D (%)[c]	D (%)[e]
Pd/SiO_2	6.7	7.8	15	13
$Pd0.5Nb/SiO_2$	6.0	--	17	
$Pd1Nb/SiO_2$	4.5 (3.9)*	5.1	22 (25)[d]	20
$Pd2.5Nb/SiO_2$	7	7.1	14	14
$Pd5Nb/SiO_2$	11.1	11.0	9	9
$Pd10Nb/SiO_2$	20.5 (14)*	11.6	5 (7)[d]	9
Pd/Nb_2O_5	4.5	4.1	22	21

[a] Particle size of Pd° calculated by Scherrer equation

[b] Particle size of Pd^0 determined by EXAFS

[c] Pd dispersion calculated by XRD for the catalysts reduced at 573 K.

[d] Pd particle size and dispersion determined by HRTEM

[e] Pd dispersion calculated by EXAFS

Table 4. Phenol conversion, HDO reaction rate and products distribution for HDO of phenol.

Catalyst	Conversion (%)	Total rate ($mmol/g_{cat}.min$)	Rate of HDO ($mmol/g_{cat}.min$)	Selectivity (%)				
						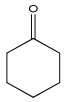	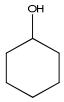	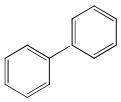
Pd/SiO_2	15.1	0.63	0.02	3.3	-	92.0	4.7	-
$Pd0.5Nb/SiO_2$	18.5	0.62	0.16	24.7	1.0	71.5	2.8	-
$Pd1Nb/SiO_2$	12.5	0.89	0.53	58.5	0.8	39.7	1.1	-
$Pd2.5Nb/SiO_2$	9.8	0.36	0.30	80.6	2.3	14.7	-	1.8
$Pd5Nb/SiO_2$	8.0	0.13	0.12	83.4	3.2	9.6	-	3.8
$Pd10Nb/SiO_2$	11.6	0.18	0.16	85.9	3.3	7.0	-	3.7
Pd/Nb_2O_5	11.4	0.98	0.82	83.0	1.7	14.9	-	0.5

Table 5. Products distribution for hydrodeoxygenation of Phenol over $PdNb/SiO_2$ catalyst after different temperature reduction ($T_{reaction}$ = 573 K, 1 atm, 5 min of TOS).

Catalyst	Reduction temperature (K)	Conversion (%)	Rate of HDO ($mmol/g_{cat}.min$)	Selectivity (%)				
						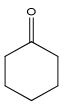	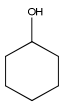	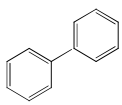
$Pd1Nb/SiO_2$	573	12.5	0.53	58.5	0.8	39.7	1.1	-
	673	12.9	0.35	49.6	1.5	46.9	2.0	-
	773	8.2	0.16	41.7	1.8	54.0	2.6	-
$Pd10Nb/SiO_2$	573	11.6	0.16	85.9	3.3	7.0	-	3.7
	673	6.7	0.07	81.4	7.9	8.7	-	2.0
	773	5.3	0.02	84.5	9.1	4.4	-	2.1

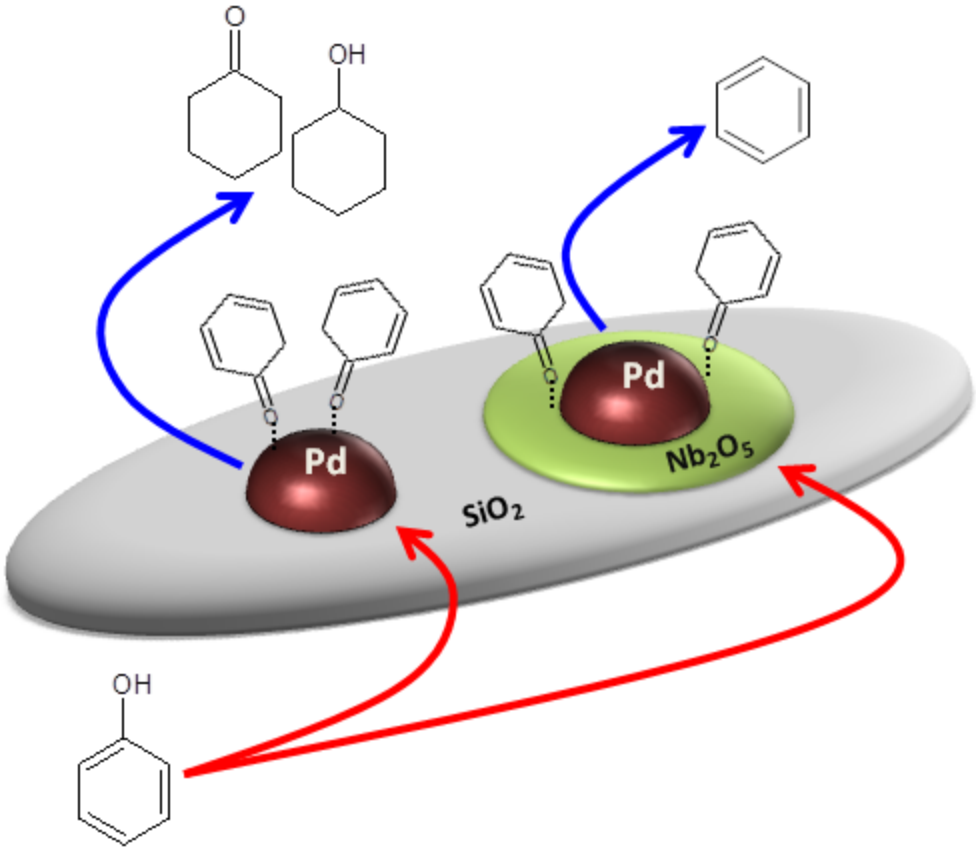
O
OH
Pd
Pd
Nb_2O_5
SiO_2
OH